Enhancing Performance of Photovoltaic Pump Systems in Remote Areas Using a Sliding Mode Technique for Maximum Power Point Tracking

Alaa Shakir Mahmood*

Middle Technical University/Institute of Technology, Baghdad, Iraq

ABSTRACT: Photovoltaic (PV) systems represent an extremely intriguing alternative in order to provide dry and semi-arid regions in remote locations with water. In this case, a maximum power point tracking (MPPT) unit that aims to regulate the PV panel connected converter duty cycle is necessary to ensure that it operates as efficiently as possible under various operating situations. This study introduces a sliding mode technique-based MPPT control unit with the goal of enhancing photovoltaic pump (PVP) system performance. It discusses this for a number of scenarios, including the presence or absence of batteries, operation under various radiation conditions, and operation in consideration of constant speed and variable load torque. The outcomes of the MATLAB simulation demonstrated that the proposed methodology is preferable compared to the incremental conductance method for the various scenarios, and it achieves better efficiency and lower voltage ripples.

1. INTRODUCTION

Focus has shifted increasingly towards power generation from renewable energy sources due to the current situation of energy sources being available to meet high-power requirements. These resources are extremely plentiful and have a significant amount of potential to close the energy gap and handle the demand that is increasing at a frightening rate. The power from the sun is abundant, clean, and ideal for the use in rural areas to utilise for water pumping [1, 2].

Because it is simple and straightforward to adopt, clean, free, and easy to maintain, solar energy generation via PV panels is widely utilised for both linked to the grid (on-grid) and not connected to the grid (off-grid) systems [3]. These and other factors have elevated solar energy systems to the status of one of the most promising energy sources, particularly in isolated places where it may be the only other option for supplying necessary electricity [4, 5].

Recent developments in semiconductor technology and the appearance of power electronics devices have significantly improved methods for energy conversion. This has greatly increased the amount of large-scale PV electricity production [3, 4]. As an interface between the PV panels and the pump, power electronics converters are used [5]. As a result, before using an inverter, the DC voltage from the PV panels must be increased. This is the first topology of the PVP drive topology, which is more practical. The only component of the second topology is a DC/AC converter, which is employed to maximise PV power and drive a motor pump. Because fewer electrical components are used in this layout, there are fewer energy losses [6].

A solar-powered irrigation pump has a number of benefits since it increases system dependability while requiring the least amount of operation and maintenance [7, 8]. It guarantees high efficiency and is cost-competitive with grid-connected water pumping systems and diesel generators [9].

Freestanding PV water pumps powered by an induction motor (IM) is currently quite common in the business and for agriculture [10, 11]. One significant problem of PV system array driven water pumps is that their water discharge changes with the change in insolation. Researchers have concentrated on the grid integration of freestanding PV system supplied water pumping systems to solve this issue [10] and other storage systems such as batteries [7].

IM control is very complex. This complexity is primarily caused by nonlinearity of its model and strongly coupled nature. A further limitation is provided by the presence of parametric uncertainty. Several nonlinear control strategies have been put out for IM drive as Backstepping control [11, 12] and sliding mode controller [3, 13]. Some use intelligent controllers like fuzzy logic [14, 15] and artificial neural networks [16, 17]. However, the most popular way is the employment of the v/f technique, which has several benefits like simplicity, convenience of use, and low cost [18, 19].

Going back to the first step of the PV pumping system, the generation of PV output power is influenced by environmental factors (such as irradiance, panel temperature), load change, and non-linear panel characteristics. So, an MPPT controller that aims to regulate the converter duty cycle is necessary to ensure that the PV array operates as efficiently as possible under various operating situations [20, 21].

The most used algorithms for MPPT are perturb and observe (P&O) and incremental conductance (IC). Numerous

* Corresponding author: Alaa Shakir Mahmood (alaa1984@mtu.edu.iq).

Nomenclature			
A	A factor related to the material from which the (PV) panel is made.	D	is the duty cycle
I_{sc}	The short-circuit current of the solar cell.	V	Voltage at both ends of the (PV) panel.
K_I	Current coefficient.	Ns	The number of cells within one plate.
G	The radiation incident on the solar panel.	e	The charge of the electron is estimated at 1.6×10^{-19}.
K	Boltzmann gas constant, 1.38×10^{-23} J/K.	E_g	Gap power of the semiconductors used in the (PV) cell.
T_c	The absolute temperature of the cell, expressed in Kelvin.	V_{oc}	The open circuit voltage of (PV).
ω_k	The speed of the reference frame.	P	A number of pole pairs.
ω_s	The synchronous speed.	L_m	Magnetizing inductance.
ω	The electric speed of the rotor.	L_s	Stator inductance.
Ω	Mechanical speed of the rotor.	L_r	Rotor inductance.
v_{sq}, v_{sd}	Are stator voltage components.	J	Rotor inertia.
i_{sq}, i_{sd}	Are stator current components.	f	Friction coefficient.
Φ_{rq}, Φ_{rd}	Are rotor flux components.	T_d	Load torque.
Φ_{sq}, Φ_{sd}	Are stator flux components.	T_{ref}	The reference temperature, expressed in Kelvin.
V_s	Is the amplitude of phase voltage (volt)		
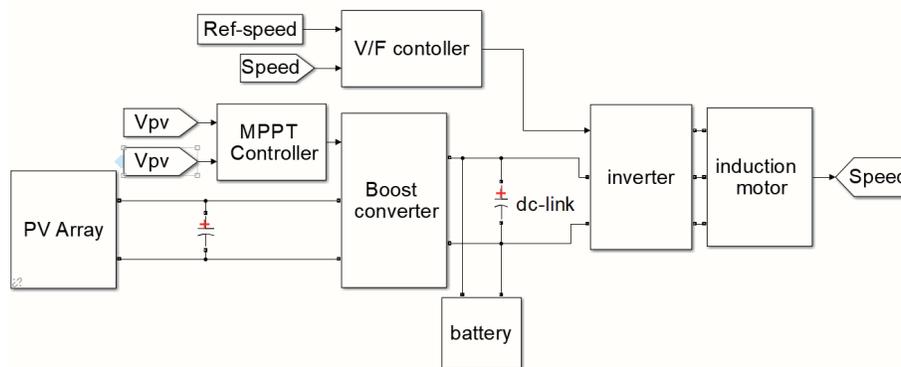
FIGURE 1. The block diagram of inverter driving IM feed by PV system.

techniques such as optimization algorithms [22, 23], fuzzy logic systems [24], and artificial neural networks [25, 26] have been previously introduced to design peak power point tracking controllers. Nonlinear control systems were also used such as backstepping [27] and sliding mode, typically used for controlling power electronic converters, which represent instances of variable structure systems. Recently, PV systems have adopted this technique [28].

In this paper, we aim to simulate a PV system feeding an IM that can operate either as a water pump, where the torque on the motor shaft is proportional to the rotational speed and the amount of water pumped, or as a constant speed variable load motor, with a battery storage system.

To control the IM, a v/f approach will be adopted, and a simple MPPT module based on the sliding mode technique will be applied.

2. CONFIGURATION OF PROPOSED SYSTEM

Figure 1 shows the structure of the proposed system, which consists of the following:

1. PV panels

2. boost converter

3. battery

4. voltage source inverter

5. IM controlled by v/f approach.

3. MATHEMATICAL SYSTEM MODEL

3.1. PV Model

3.1.1. Modelling PV Cell

The PV panel is primarily made up of PV cells, which are semiconductor materials. Connectors are also included as protection
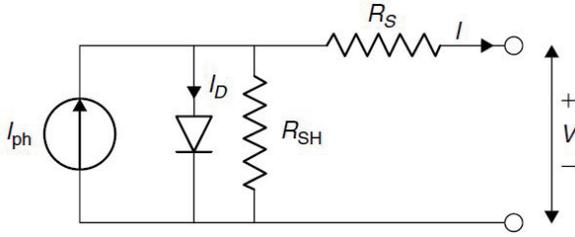
FIGURE 2. Equivalent circuit for a single PV cell model.

FIGURE 3. The structure of the boost chopper.

and support parts. The electrical circuit model, as seen in Figure 2, typically serves as a representation of the PV cell [29, 30].

The mathematical model of PV cell is given as:

$$I = [I_{sc} + k_I(T_c - T_{ref})]\frac{G}{1000} - I_D - \frac{V + IR_s}{R_{sh}} \quad (1)$$

$$I_D = I_s \left\{ \exp\left[\frac{e(V + IR_s)}{N_s A k T_c}\right] - 1 \right\} \quad (2)$$

$$I_s = \left(\frac{I_{sc}}{\exp\left\{\frac{eV_{oc}}{N_s k A T_c} - 1\right\}}\right)\left(\frac{T_c}{T_{ref}}\right)^3$$

$$\exp\left\{\frac{e \cdot E_g}{kA}\left[\frac{1}{T_{ref}} - \frac{1}{T_c}\right]\right\} \quad (3)$$

Whereas:

3.1.2. Boost Converter Model

To extract the most power possible from PV, the DC-DC converter must be managed. The boost chopper model used in this paper is depicted in Figure 3, and its dynamic model is provided below [31]:

$$\frac{V_o}{V_s} = \frac{1}{1 - D} \quad (4)$$

$$\frac{dI_s}{dt} = \frac{-(1 - D)V_o + V_s}{L} \quad (5)$$

$$\frac{dV_o}{dt} = \frac{(1 - D)I_s - I_o}{C} \quad (6)$$

3.2. IM Drive System Model

3.2.1. IM Drive System Model

The following equations represent a 3-ph IM mathematically in a reference d-q frame rotating at ω_k [32]:

$$\frac{di_{sd}}{dt} = -a_5 i_{sd} + \omega_k i_{sq} + a_3 \Phi_{rd} + a_4 \omega \Phi_{rq} + b v_{sd} \quad (7)$$

$$\frac{di_{sq}}{dt} = -\omega_k i_{sd} - a_5 i_{sq} - a_4 \omega \Phi_{rd} + a_3 \Phi_{rq} + b v_{sq} \quad (8)$$

$$\frac{d\Phi_{rd}}{dt} = a_2 i_{sd} - a_1 \Phi_{rd} + (\omega_k - \omega)\Phi_{rq} \quad (9)$$

$$\frac{d\Phi_{rq}}{dt} = a_2 i_{sq} - (\omega_k - \omega)\Phi_{rd} - a_1 \Phi_{rq} \quad (10)$$

$$\frac{d\omega}{dt} = \frac{p}{J}(G\Phi_{rd}i_{sq} - G\Phi_{rq}i_{sd} - T_d) - \frac{f}{J}\omega \quad (11)$$

$$\Phi_{s\alpha} = \int (v_{s\alpha} - i_{s\alpha}R_s) \quad (12)$$

$$\Phi_{s\beta} = \int (v_{s\beta} - i_{s\alpha}R_s) \quad (13)$$

$$|\Phi_s| = \sqrt{\Phi_{sd}^2 + \Phi_{sd}^2} \quad (14)$$

$$a_1 = \frac{R_r}{L_r}, \quad a_2 = \frac{L_m R_r}{L_r}, \quad a_3 = \frac{L_m R_r}{\sigma L_s L_r^2},$$

$$a_4 = \frac{L_m}{\sigma L_s L_r}, \quad a_5 = \frac{L_r^2 R_s + L_m^2 R_r}{\sigma L_s L_r^2},$$

$$b = \frac{1}{\sigma L_s}, \ G = \frac{P L_m}{L_r}, \ \sigma = 1 - \frac{L_m^2}{L_s L_r}, \ \omega = P\Omega$$

The relation (15) (park transformer) is used to convert the electrical signals from a, b, c frame to d, q frame rotating at ω_k or vice versa [33, 34].

$$\begin{bmatrix} X_d \\ X_q \end{bmatrix} = \sqrt{3/2}\begin{bmatrix} \cos(\theta_k) & \cos(\theta_k - \frac{2\pi}{3}) & \cos(\theta_k + \frac{2\pi}{3}) \\ -\sin(\theta_k) & -\sin(\theta_k - \frac{2\pi}{3}) & -\sin(\theta_k + \frac{2\pi}{3}) \end{bmatrix}$$

$$\begin{bmatrix} X_a \\ X_b \\ X_c \end{bmatrix} \quad (15)$$

3.2.2. Voltage Inverter

The voltage inverter shown in Figure 4 consisting of six transistors converts the DC voltage provided by the output of the boost converter into an AC voltage used to feed the IM. The voltage inverter feeding the IM is driven using sinusoidal pulse width modulation (SPWM) technology, as shown in Figure 4.

Figure 5 depicts the signal creation based on a comparison of the triangle waveform and the three-phase control waveform.
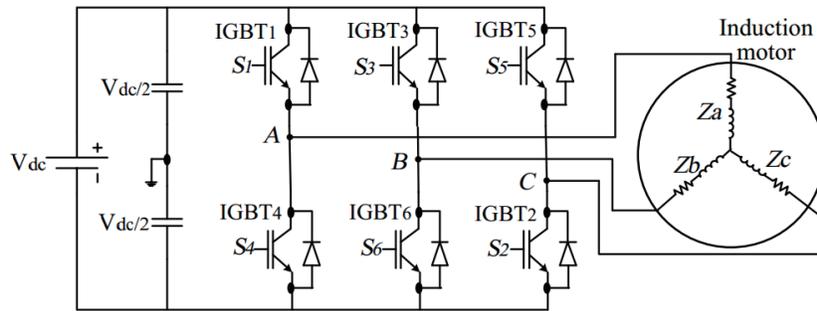
FIGURE 4. Structure of inverter feeding the indiction motor.
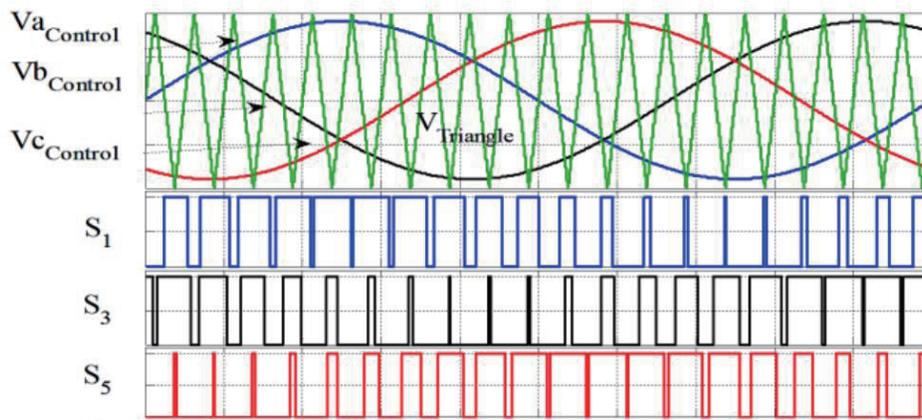
FIGURE 5. SPWM technology for 3-ph inverter.
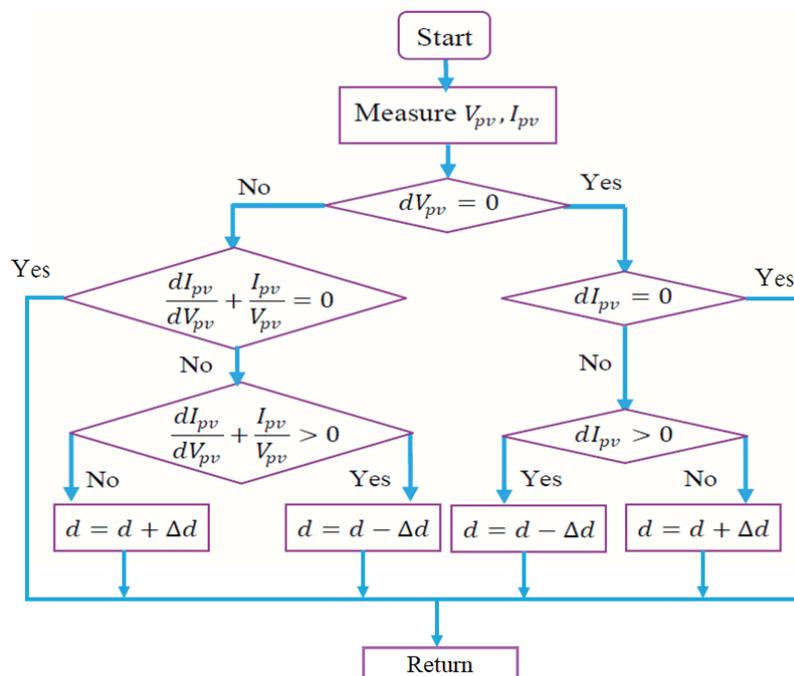
FIGURE 6. The flowchart of INC algorithm.
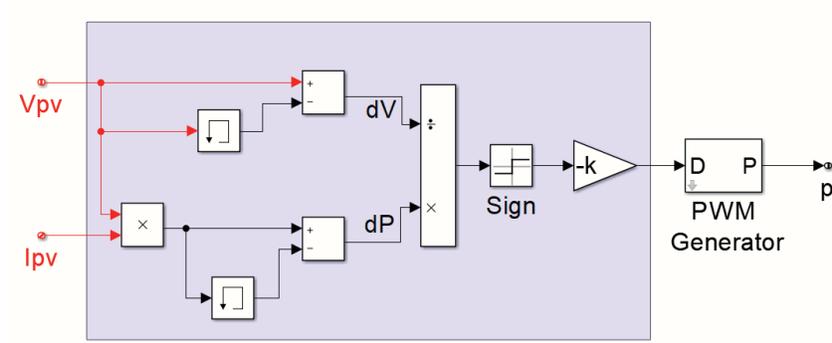
FIGURE 7. The block diagram of the SM MPPT controller.
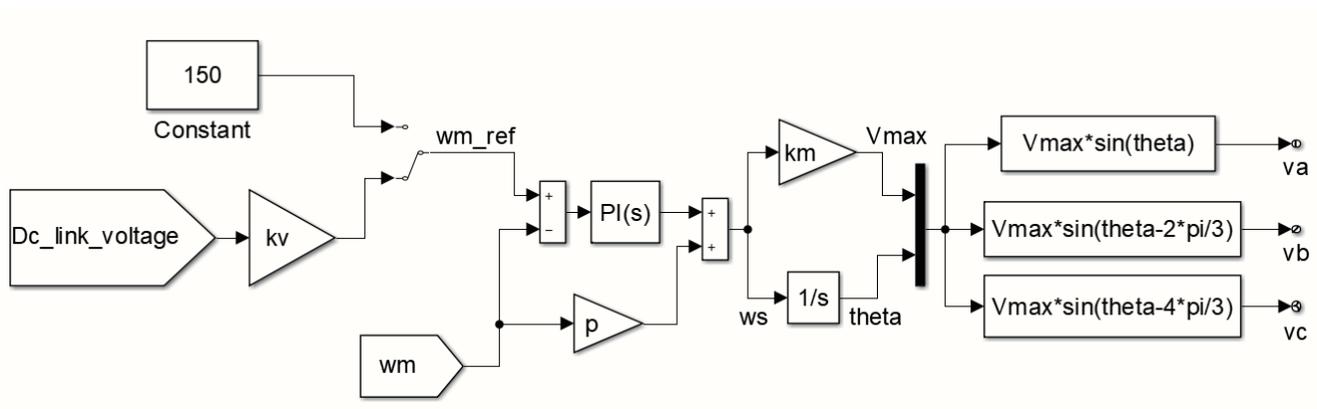
FIGURE 8. The block diagram of v/f controller and reference speed adjustment mechanism.
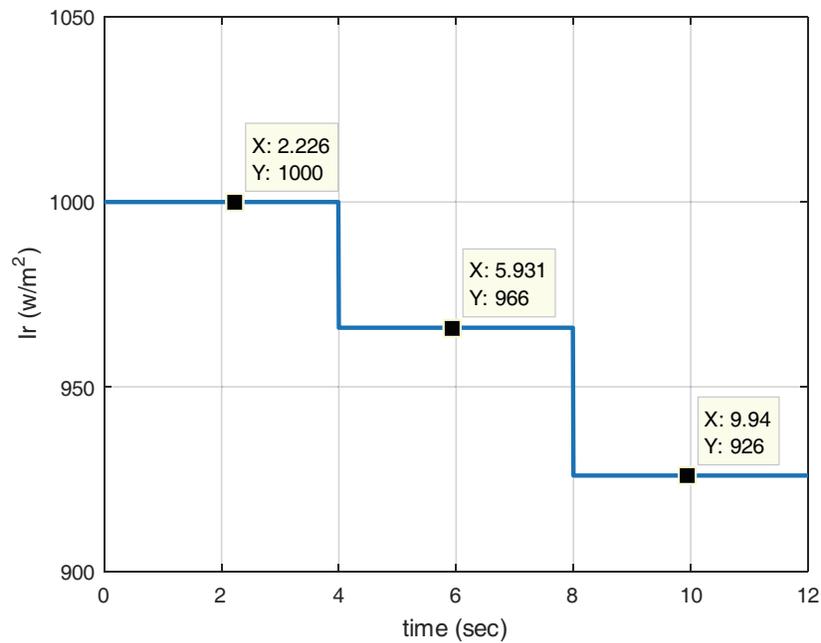
FIGURE 9. The photoelectric radiation profile.

TABLE 1. The number of panels used and the parameters of each panel.

Parallel strings	15
Series-connected modules per string	20
Maximum Power (W)	152.4
Open circuit voltage Voc (V)	21.2
Voltage at maximum power point Vmp (V)	17.23
Short-circuit current Isc (A)	9.27
Current at maximum power point Imp (A)	8.85
Maximum Power all panels (W)	45720
Voltage all panels (V)	344.6
Current all panels (A)	132.75
Total number of panels	300 Panels
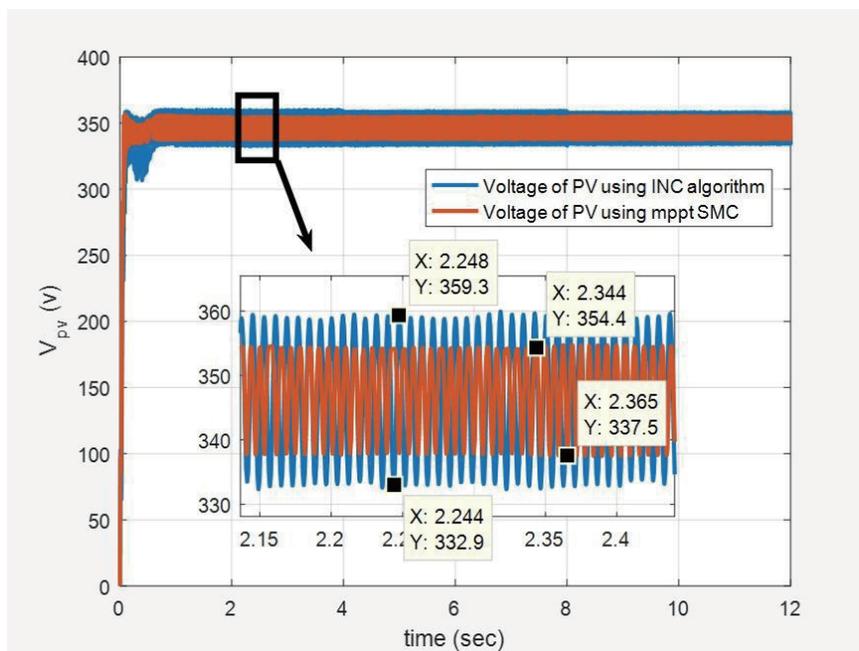
FIGURE 10. The voltage changes at the terminals of the PV panels.

4. CONTROL SYSTEMS DESIGN

4.1. MPPT Control

Only 12% to 25% of solar energy is transformed into electricity by PV panels, which have a high initial cost of installation and poor energy output. Researchers have investigated a number of ways, including using an MPPT controller and printed thin PV cells, to boost the overall quantity of electric energy produced [25]. An MPPT unit consists of a power converter and an embedded electrical system with a control algorithm. Every PV installation is designed to absorb the maximum energy feasible in the present under all imaginable operating and environmental conditions [21, 25].

The maximum power point (MPP) of a PV cell's current-voltage curve can be located using an open-loop control method called the incremental conductance (INC) algorithm. This is

based on the PV power derivative with respect to PV voltage, which is equal to zero at MPP, negative to the right of MPP, and positive to the left of MPP [28]. Figure 6 is an illustration of the INC algorithm flowchart.

In the second step, a simple and efficient MPPT control system is designed, based on the sliding mode technology. By using sliding mode technique, the system is regulated by a control unit such that the states of the system are always headed for a sliding surface. The error e of the state is used to define the sliding surface. The control signal Uc of the system is chosen based on the error trajectory's distance from the sliding surface and its rate of changes. To change the state trajectory towards the equilibrium surface and keep it there, choose a switching control method as follows [32]: Return

$$U_c = -k\text{sign}(s) \tag{16}$$
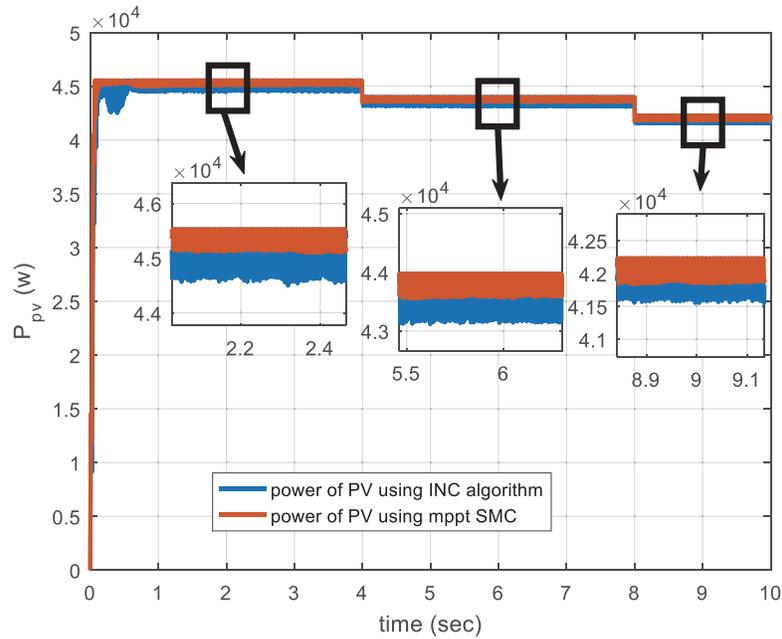
FIGURE 11. The power of PV.
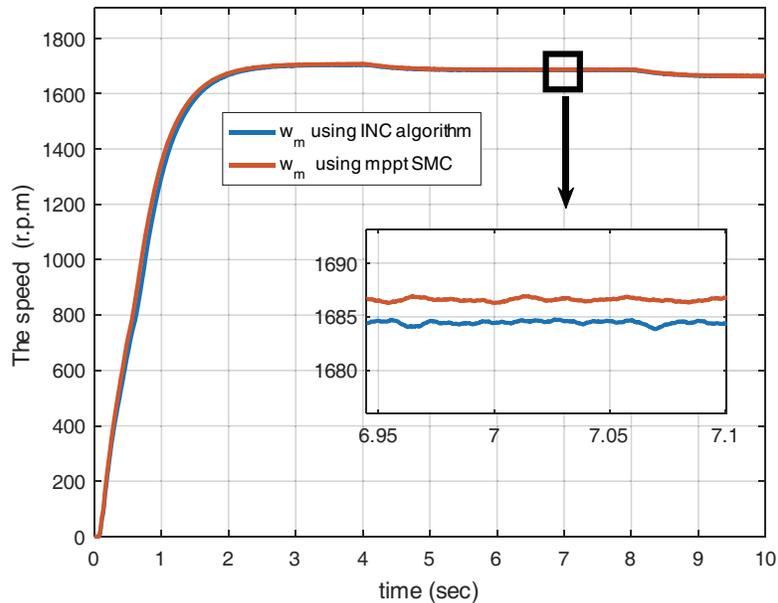
FIGURE 12. The speed of the pump.

In PV systems, the MPP is achieved when ($\frac{dP}{dV} = 0$) [21], where:

$$\frac{dP}{dV} = \frac{d(VI)}{dV} = I\frac{dV}{dV} + V\frac{dI}{dV} = 0 \text{ at the MPP} \quad (17)$$

Therefore, to implement a sliding mode MPPT controller, the control law is given in (18) as follows:

$$U_c = -k\text{sign}\left(\frac{dP}{dV}\right) \quad (18)$$

where U_c in (18) denotes the duty cycle for the boost converter. Figure 7 shows the block diagram of the sliding mode (SM) MPPT controller.

4.2. V/F Control of an IM

Scalar control and vector control are the two main types of control systems used in IM drive [35]. By maintaining a constant voltage to frequency ratio, the scalar control offers an easy-to-use method of managing the speed of an IM. In the steady-state, this technique offers a good response [36, 37].
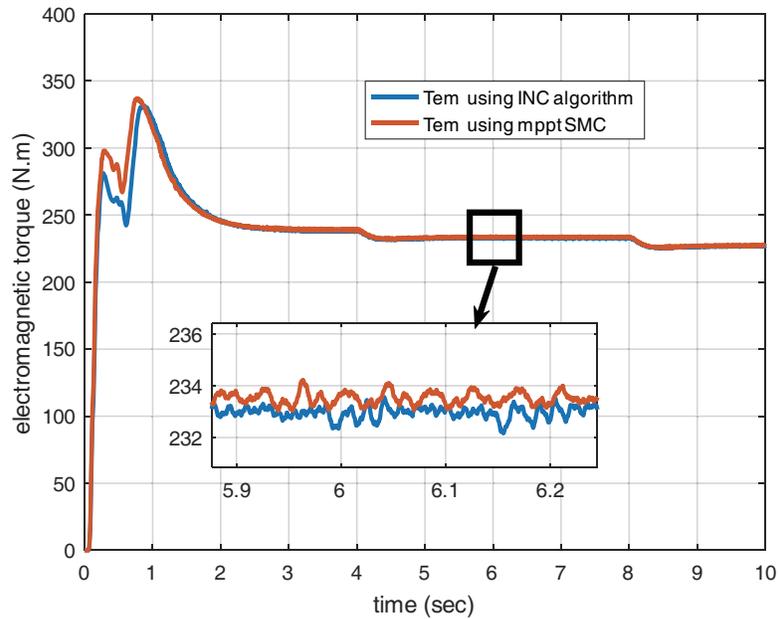
FIGURE 13. The electromagnetic torque of the pump.
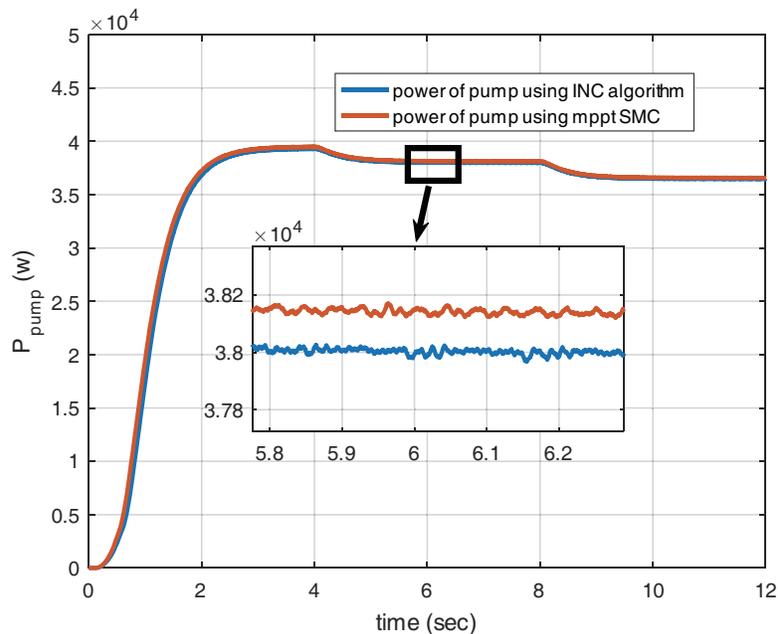
FIGURE 14. The mechanical power of pump.

The goal of v/f control is to maintain a constant voltage/frequency ratio (v/f), which keeps the magnetic flux (Φ_s) in the air gap at its rated level. To achieve this, the following relationship between voltage and frequency must be achieved [15, 35]:

$$\frac{V_s}{\omega_s} = \Phi_s = k_m \tag{19}$$

where ω_s is the frequency (rad/sec). k_m is the ratio of V_s to ω_s.

Figure 8 shows the block diagram of the v/f control system, where the reference speed is determined according to a pattern determined by the designer, either a fixed value is chosen, or it is determined according to the dc link voltage related to the power coming from the PV panels, as the dc link voltage increases with increase of this power, and thus the motor speed increases or vice versa.

$$k_v = \frac{\Omega_{nominal}}{V_{dc}nominal} = \frac{170}{780} = 0.21795 \, \text{rad} \cdot \text{v/sec}.$$
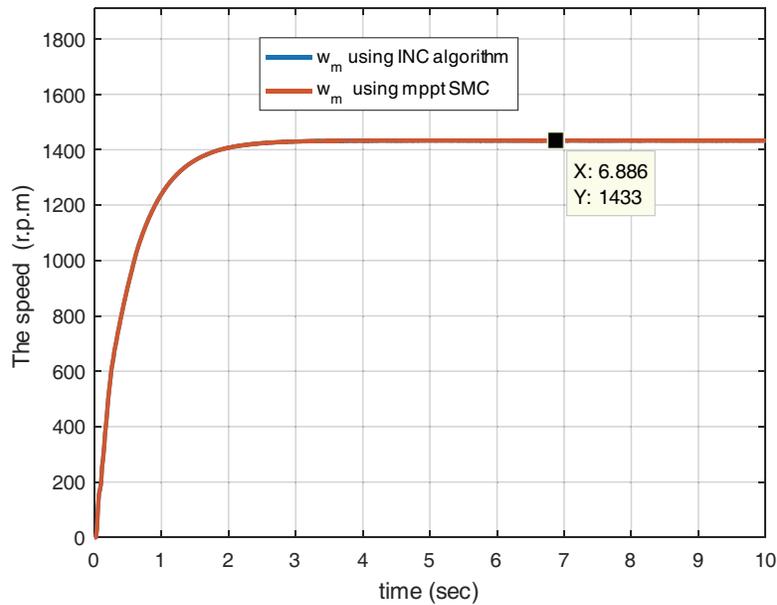
FIGURE 15. The rotational speed of the pump.

TABLE 2. Simulation results for the first scenario (pump operating without battery).

	PV power (kw)	Speed pump (r.p.m)	electromagnetic torque (N.m)	Pump power (Kw)
$Ir = 1000\,\text{w/m}^2$				
SMC	45.33	1706	239.4	39.43
INC	45.15	1703	238.5	39.25
$Ir = 966\,\text{w/m}^2$				
	PV power (kw)	Speed pump (r.p.m)	electromagnetic torque (N.m)	Pump power (Kw)
SMC	43.84	1688	233.8	38.17
INC	43.69	1686	233.1	38.01
$Ir = 926\,\text{w/m}^2$				
	PV power (kw)	Speed pump (r.p.m)	electromagnetic torque (N.m)	Pump power (Kw)
SMC	42.06	1664	227.4	36.57
INC	41.95	1662	226.7	36.48

4.3. Design of Pump

When the motor operates as a pump, the load torque is proportional to the rotational speed according to the following relationship [19]:

$$T_d = k_{pump}\Omega^2 \qquad (20)$$

where $k_{pump} = \frac{T_{d_{nominal}}}{\Omega_{nominal}^2} = \frac{200}{170^2} = 0.0069\,\text{N·m}/\left(\frac{\text{sec}}{\text{rad}}\right)^2$.

5. SIMULATION RESULTS

The photoelectric radiation profile is shown in Figure 9, and the temperature value was set at 25°C. The parameters of panels is shown in Table 1.

The pump's output power is 34 kW. Consequently, the number of panels was selected to ensure that their power is appropriate for the pump, accounting for losses and efficiency. A total of 300 panels were chosen, with a collective capacity of 45 kW. These panels are distributed among 15 series, each comprising 20 panels, to achieve an approximate voltage of 345 V. Using a DC-DC boost converter, the final output DC voltage is increased to approximately 780 V to match the input DC voltage required by the inverter supplying power to the pump.

5.1. Case 1

To test the efficiency of the proposed control system, the system was initially operated without batteries. In this setup, the reference motor speed was determined based on the DC link
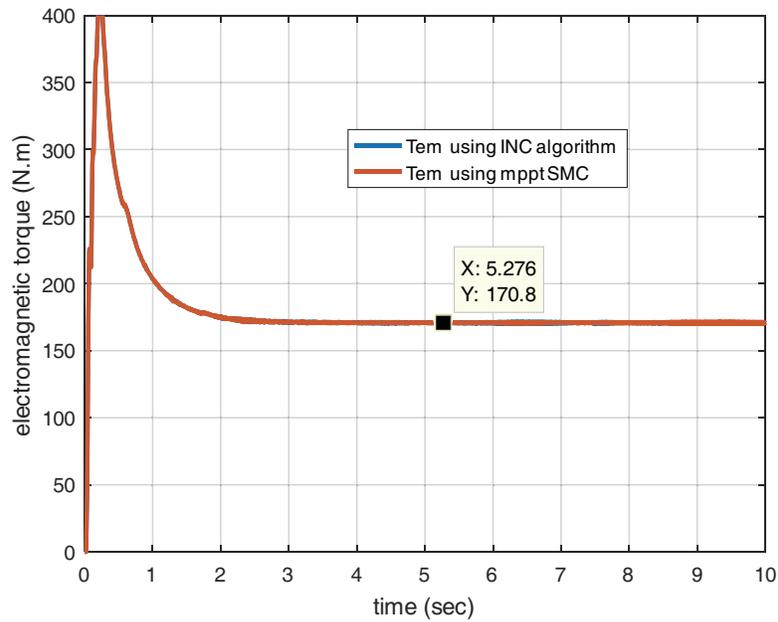
FIGURE 16. The electromagnetic torque in the pump.
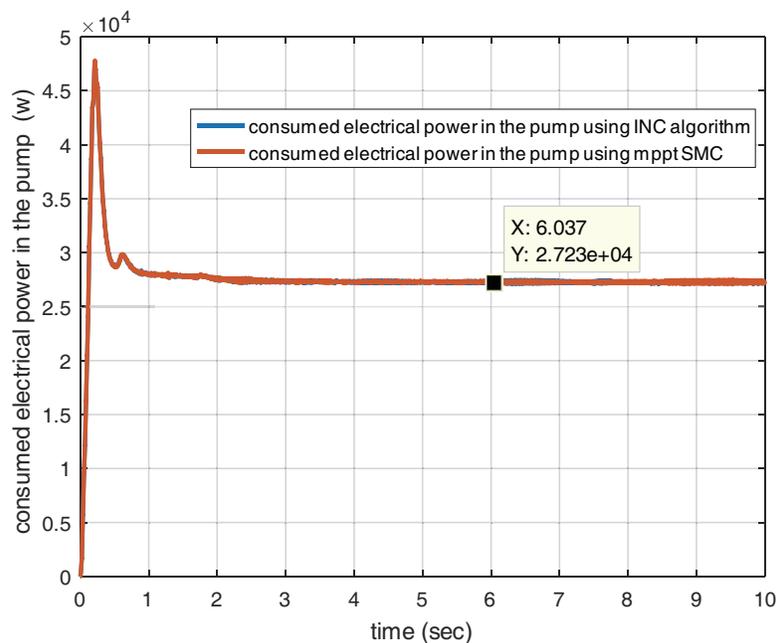
FIGURE 17. The electric power consumed by the pump.

voltage between the boost converter and the inverter that feeds the motor, which is related to the power drawn from the PV panels. Figure 10 shows the voltage changes at the terminals of the PV panels. Figure 11 shows the electrical power extracted from PV panels with changes in the intensity of solar irradiation. Figure 12 shows the pump speed. Figure 13 shows the electromagnetic torque of the PV pump, and Figure 14 shows the mechanical power of the pump.

Considering that the temperature is 25 degrees Celsius, then the terminal voltage of the panels must be 344.6 volts, Refer-

ring to Figure 10, which shows that the panels voltage fluctuates within a range of [333–360]v when using an incremental conductivity controller, while it is observed that it fluctuates within a range of [337–355]v when using a sliding mode controller, it can be said that the latter controller achieves greater performance and stability for the system.

With the decrease in the value of photoelectric radiation, the power drawn from the panels will generally decrease, as shown in Figure 11, however, it is noted from Figure 11 that the SMC controller achieves MPP tracking with high efficiency and the
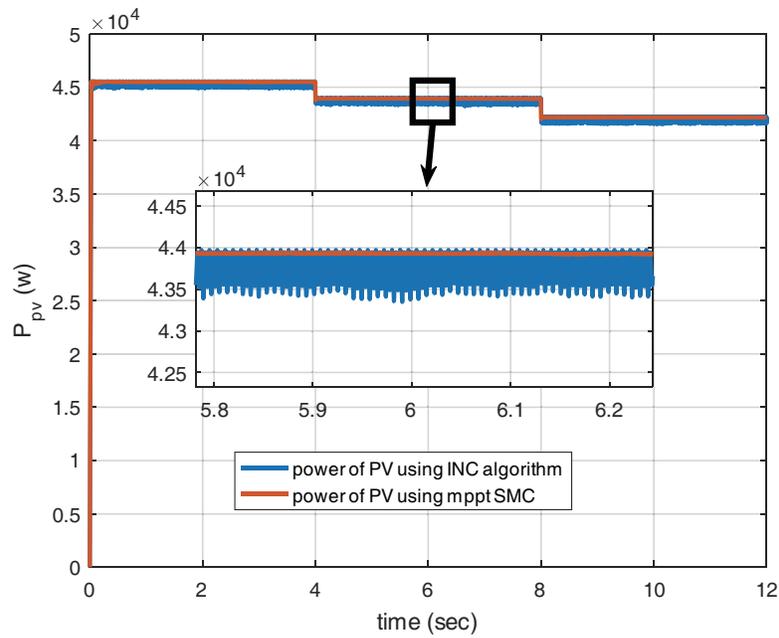
FIGURE 18. The power provided by the PV panels.
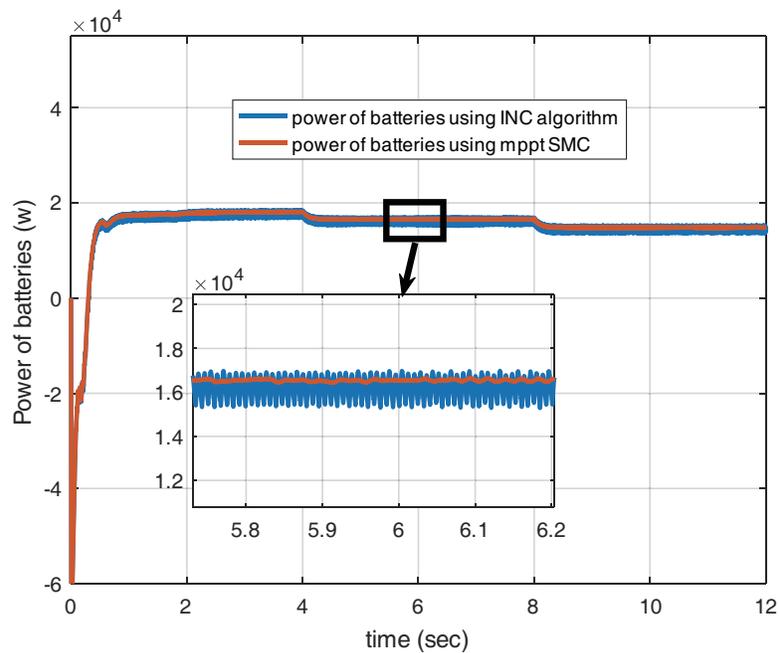
FIGURE 19. The power charged to the batteries.

maximum power point, where the power is greater with fewer ripples.

In Figure 13, the results show that the electromagnetic torque of the pump changes with changes in the intensity of solar irradiation and changes in the electrical power extracted from the PV panels.

Table 2 shows the power values corresponding to changes in solar irradiation intensity and their effect on the performance of the PV pump (speed, torque, and pump power).

The results presented in Table 2 demonstrate the superiority of the sliding mode algorithm, as it is noted that with the change in solar radiation values, the power obtained from the panels using this technique is always greater, and in return, the rotational speed and torque of the pump are greater, and as a result, greater pumping capacity.

5.2. Case 2

In the second scenario, the pump will operate at a constant rotational speed, and therefore a battery (energy storage system, ESS) must be available to provide the necessary power to oper-

TABLE 3. Simulation results for the first scenario (pump operating at constant speed).

$Ir = 1000\,\text{w/m}^2$, Speed pump $= 1433$ r.p.m, Tem $= 171$ N·m		
	PV power (kw)	power charged to the batteries (kw)
SMC	45.50	18.05
INC	45.26	17.72
$Ir = 966\,\text{w/m}^2$, Speed pump $= 1433$ r.p.m, Tem $= 171$ N·m		
	PV power (kw)	power charged to the batteries (kw)
SMC	43.93	16.54
INC	43.70	16.26
$Ir = 926\,\text{w/m}^2$, Speed pump $= 1433$ r.p.m, Tem $= 171$ N·m		
	PV power (kw)	power charged to the batteries (kw)
SMC	42.17	14.85
INC	41.95	14.58
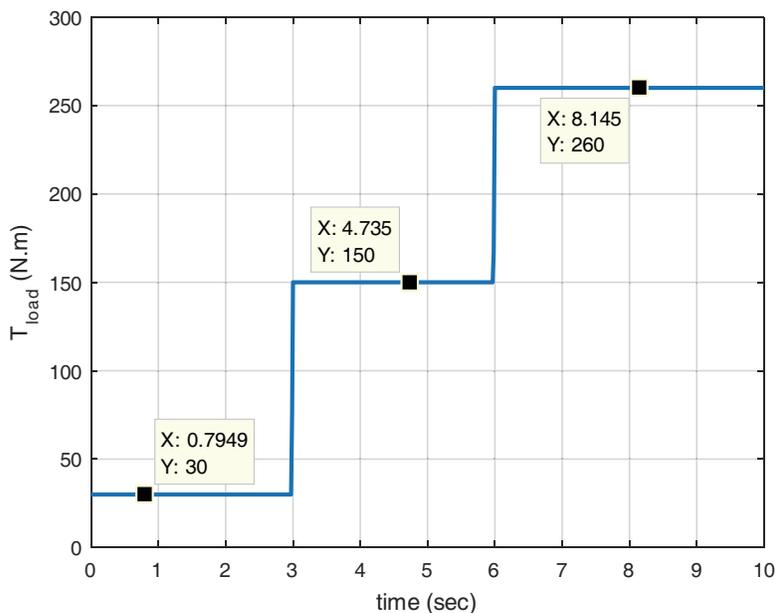
FIGURE 20. The load torque changes.

ate according to this mode, and to maintain the stability of the operate of the motor (pump) despite change of solar radiation.

Figures 15 and 16 show the rotational speed of the pump and electromagnetic torque, respectively, and Figure 17 shows the electric power consumed by the pump.

Figures 18 and 19 show the power provided by the PV panels and the power charged to the batteries, respectively.

Figures 15 and 16 show that the pump operates at a constant speed and torque. The speed is equal to 1443 r.p.m, and the torque is equal to 171 N·m, so the power consumed by the pump remains constant as shown in Figure 17 and is equal to 27.16 Kw. It is clear that the power consumed by the pump is less than the power provided by the PV panels, as the surplus

power is stored in the batteries as shown in Figure 18. From Figures 19 it is possible to note the superiority of the sliding mode approach in achieving greater power from PV and charging batteries with greater power, regardless of the changes occurring in solar radiation. This is shown in Table 3.

5.3. Case 3

In the third scenario, the speed will be regulated at a fixed value equal to 1600 r.p.m as the load torque changes as shown in Figure 20, knowing that solar radiation is a fixed value and equal to 800 w/m^2. Figures 21–23 show the motor rotation speed, electromagnetic torque, and the power drawn by the motor, respectively. Figure 24 shows the energy derived from PV panels,
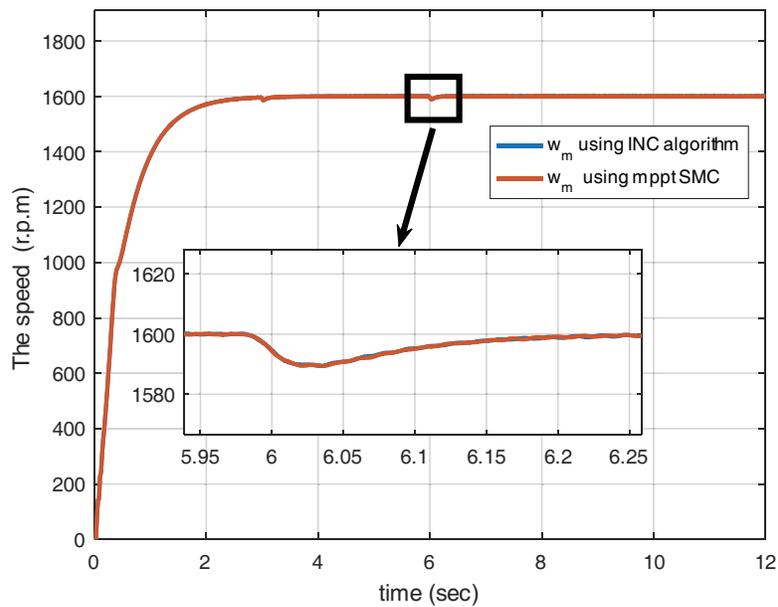
FIGURE 21. The rotational speed of the pump.
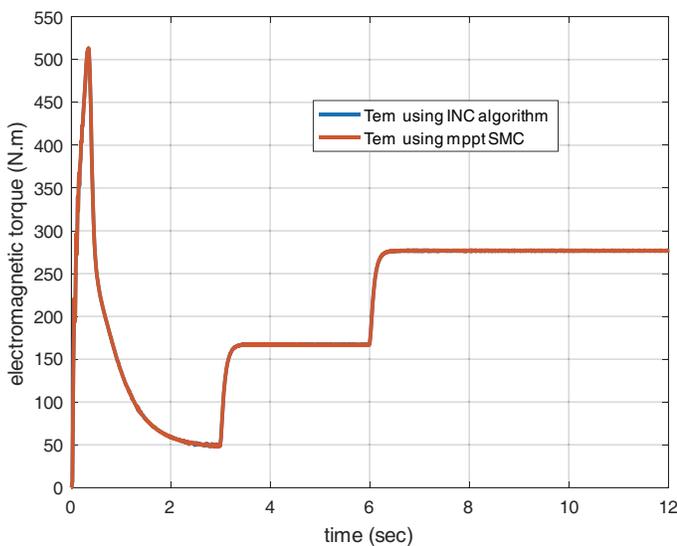
FIGURE 22. The electromagnetic torque in the pump.
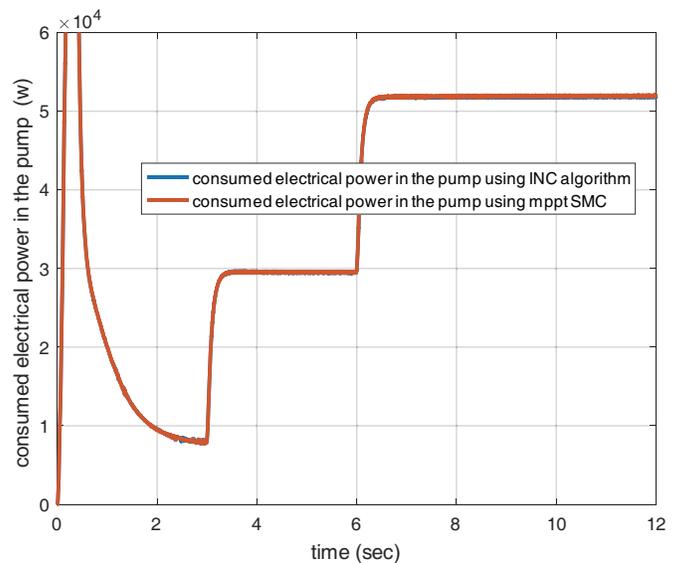
FIGURE 23. The electric power consumed by the motor.

and Figure 25 shows the battery energy for both MPPT technologies.

It can be seen from Figure 21 that the drive system achieves satisfactory and good performance in pursuing the required reference speed regardless of the value of the load torque applied to the engine, as the speed value is equal to 1600 rpm. From Figure 22, it is noted that the electromagnetic torque is initially large in value, and this is normal due to the necessity of generating a starting torque for the motor, which make it draw large electrical power during the start-up period. This is what can be observed from Figure 23. After exceeding the motor start-up period, the value of the electromagnetic torque becomes proportional to the value of the torque applied to it, and thus the

value of the input energy decreases due to the decrease in the value of the applied torque and increases as it increases.

From Figure 24, it can also be noted that the power derived from the panels is greater when using SM-MPPT controller, and from Figure 25 it can be noted that the battery provides the necessary energy for the motor to start during the start period (with the presence of load torque), then the battery begins charging after the power drawn by the motor decreases, as long as the power provided by the (PV) panels is greater than the power needed by the motor.

At moment 6 sec, the power needed by the motor becomes greater than the power provided by the PV panels, and then the battery begins to discharge to provide the motor with the necessary power, but it is noted that the discharged power is
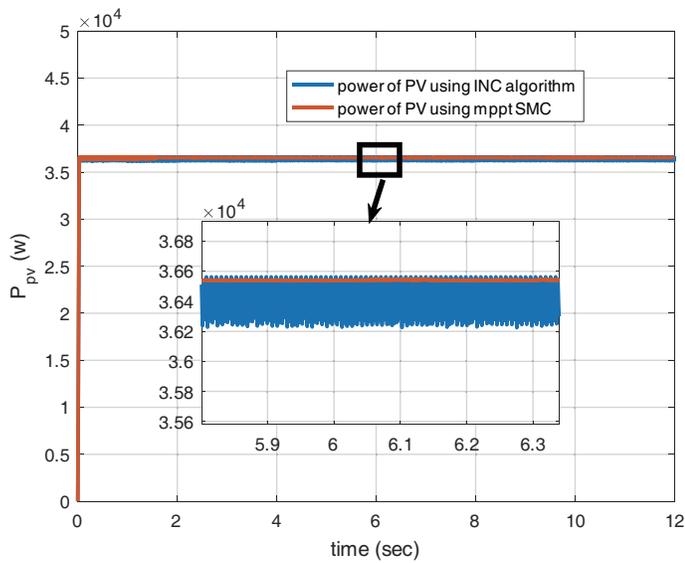
FIGURE 24. The power provided by the PV panels.
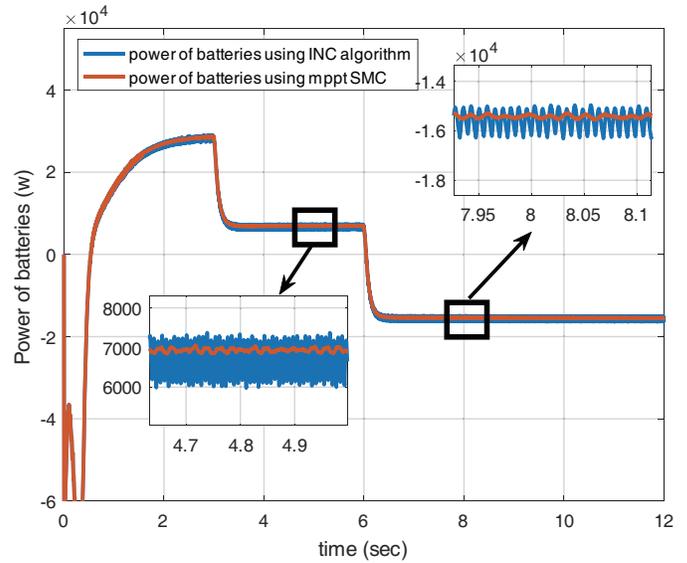
FIGURE 25. The power charged/discharged to/from the batteries.
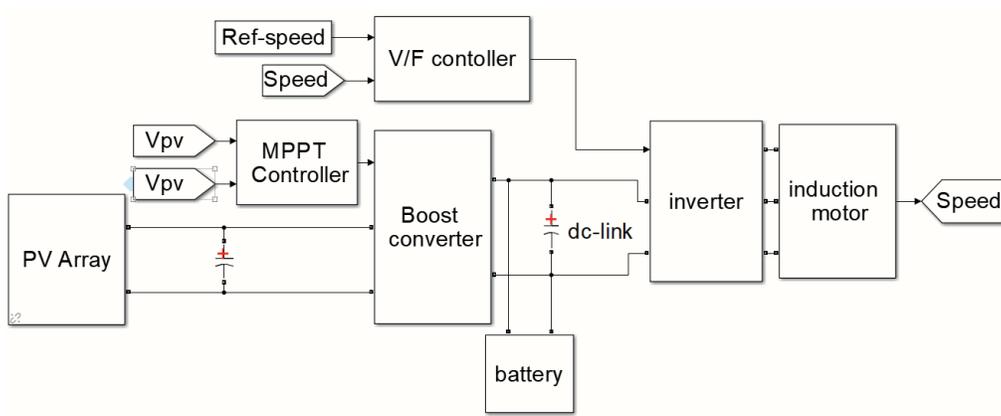
FIGURE 26. Final diagram of the PV pumping system.

TABLE 4. Simulation results for the third scenario (the motor operating at constant speed and variable load torque).

$Ir = 800\,\text{w/m}^2$, Speed pump $= 1600$ r.p.m, load torque $= 30$ N·m		
	PV power (kw)	power of the batteries (kw)
SMC	36.54	28.6
INC	36.41	28.12
$Ir = 800\,\text{w/m}^2$, Speed pump $= 1600$ r.p.m, load torque $= 150$ N·m		
	PV power (kw)	power charged to the batteries (kw)
SMC	36.54	6.9
INC	36.41	6.6
$Ir = 800\,\text{w/m}^2$, Speed pump $= 1600$ r.p.m, load torque $= 260$ N·m		
	PV power (kw)	power charged to the batteries (kw)
SMC	36.54	-15.4
INC	36.41	-15.7

less when SM-MPPT controller is used, as shown in Figure 25. Table 4 shows a summary of the results of the third scenario.

The results in Tables 2, 3, and 4 show that the electrical energy provided by the photovoltaic panels is greater if a sliding mode controller is used for the same value of the optical energy transmitted to these panels. This means that it makes the generation system more efficient.

Figure 26 shows the final block diagram of the photovoltaic pumping system, which was applied in three test cases with a slight difference. In the first case, there is no battery, while in the last two cases, there is a battery.

6. A REVIEW OF THE RESULTS FOR THE SCENARIOS STUDIED DURING THE RESEARCH

The experiences and results drawn from the previous three scenarios can be summarized as follows:

1. The PV pump operates without batteries, where the reference motor speed is determined based on the power generated from the PV panels under varying radiation conditions. It was observed that using the SM MPPT controller contributes to the ability to operate at higher rotation speeds, thus increasing mechanical power.

2. The pump operates at a constant rotational speed in the presence of a battery to provide the necessary power for operation in this mode and to maintain motor (pump) stability despite changes in solar radiation. It was noticed that the energy charged to the batteries is higher when using the SM MPPT controller.

3. The pump operates at a constant speed with variable load torque, in the presence of a battery. It was observed that the power charged to the batteries is higher when using the SM MPPT controller in the event of an excess of electrical power, while the power drawn from the batteries is lower when there is a shortage of power from the panels.

7. CONCLUSION

This research aims to improve the performance of photovoltaic pumping (PVP) systems based on induction motors and to benefit from solar energy and convert it into electrical energy for the use in irrigation of remote areas. The study explores scenarios involving pump operation (PV) with/without batteries, constant rotation speed with constant/variable torque as solar irradiation intensity changes. Simulations in MATLAB/Simulink have shown that sliding-mode MPPT improves efficiency and reduces voltage ripples, promising advanced solutions for water supply in challenging environmental conditions. It is possible to benefit from this study and apply it in various fields that use alternating current motors, such as electric cars, air conditioning and refrigeration systems, and industrial applications.

REFERENCES

[1] Akarne, Y., A. Essadki, T. Nasser, and H. Laghridat, "Modelling and control of a grid-connected AC microgrid with the integration of an electric vehicle," *Clean Energy*, Vol. 7, No. 4, 707–720, 2023.

[2] Mahmood, A. S., M. Teke, R. K. Ibrahim, A. H. Ali, A. A. Abdulrazzaq, and M. M. Kareem, "Tracking the MPP of a PV system using an advanced fuzzy logic control technique," in *2022 Second International Conference on Advances in Electrical, Computing, Communication and Sustainable Technologies (ICAECT)*, 1–7, 2022.

[3] Rai, R., S. Shukla, and B. Singh, "Sensorless field oriented SMCC based integral sliding mode for solar PV based induction motor drive for water pumping," *IEEE Transactions on Industry Applications*, Vol. 56, No. 5, 5056–5064, 2020.

[4] Genc, N., "PV based V/F controlled induction motor drive for water pumping," *International Journal on Technical and Physical Problems of Engineering (IJTPE)*, Vol. 12, No. 45, 2020.

[5] Altimania, M. R., N. A. Elsonbaty, M. A. Enany, M. M. Gamil, S. Alzahrani, M. H. Alraddadi, R. Alsulami, M. Alhartomi, M. Alghuson, F. Alatawi, *et al.*, "Optimal performance of photovoltaic-powered water pumping system," *Mathematics*, Vol. 11, No. 3, 731, 2023.

[6] Zhu, R., G. D. Carne, F. Deng, and M. Liserre, "Integration of large photovoltaic and wind system by means of smart transformer," *IEEE Transactions on Industrial Electronics*, Vol. 64, No. 11, 8928–8938, 2017.

[7] Shukla, S., B. Singh, P. Shaw, A. Al-Durra, T. H. El-Fouly, and E. F. El-Saadany, "A new analytical mppt-based induction motor drive for solar PV water pumping system with battery backup," *IEEE Transactions on Industrial Electronics*, Vol. 69, No. 6, 5768–5781, 2021.

[8] Ferreira Filho, J. R. M., F. R. F. Mendes, J. R. B. Sousa, C. M. S. Medeiros, and I. R. Sousa, "Photovoltaic panel based pumping system: a solution without batteries," *IEEE Latin America Transactions*, Vol. 16, No. 2, 514–520, 2018.

[9] Ramos, J. S. and H. M. Ramos, "Solar powered pumps to supply water for rural or isolated zones: A case study," *Energy for Sustainable Development*, Vol. 13, No. 3, 151–158, 2009.

[10] Varshney, A., U. Sharma, and B. Singh, "An intelligent grid integrated solar PV array fed RSM drive-based water pumping system," *IEEE Transactions on Industry Applications*, Vol. 57, No. 2, 1818–1829, 2020.

[11] Saoudi, A., S. Krim, and M. F. Mimouni, "Enhanced intelligent closed loop direct torque and flux control of induction motor for standalone photovoltaic water pumping system," *Energies*, Vol. 14, No. 24, 8245, 2021.

[12] Madark, M., A. Ba-Razzouk, and M. E. Malah, "Linear and nonlinear controllers of a solar photovoltaic water pumping system," *Bulletin of Electrical Engineering and Informatics*, Vol. 9, No. 5, 1861–1872, 2020.

[13] Veselic, B., B. Perunicic-Drazenovic, and C. Milosavljevic, "High-performance position control of induction motor using discrete-time sliding-mode control," *IEEE Transactions on Industrial Electronics*, Vol. 55, No. 11, 3809–3817, 2008.

[14] Belgacem, A., Y. Miloud, M. Mostefai, and F. Belgacem, "Fuzzy logic direct torque control of induction motor for photovoltaic water pumping system," *International Journal of Power Electronics and Drive Systems (IJPEDS)*, Vol. 13, No. 3, 1822–1832, 2022.

[15] Abd Ali, J., M. A. Hannan, A. Mohamed, and M. G. M. Abdolrasol, "Fuzzy logic speed controller optimization approach for induction motor drive using backtracking search algorithm," *Measurement*, Vol. 78, 49–62, 2016.

[16] Idrissi, Y. E. A., K. Assalaou, L. Elmahni, and E. Aitiaz, "New improved MPPT based on artificial neural network and PI controller for photovoltaic applications," *International Journal of Power Electronics and Drive Systems*, Vol. 13, No. 3, 1791,

2022.

[17] Maarouf, S., A. Ksentini, R. Kebbache, G. Boukerche, *et al.*, "Improved artificial neural network design for MPPT grid-connected photovoltaic systems," *The Scientific Bulletin of Electrical Engineering Faculty*, Vol. 22, No. 2, 26–31.

[18] Tayebi, A., M. Brahami, M. Yaichi, and B. Abdelkader, "Design and implementation of SVM for three phase inverter fed an induction motor for photovoltaic stand-alone pumping system," in *2019 7th International Renewable and Sustainable Energy Conference (IRSEC)*, 1–6, 2019.

[19] Esmeail, A. A. S., S. Oncu, and N. Altin, "An MPPT controlled three phase PV supplied water pumping system," in *Proc. 13th Int. Conf. Electron. Comput. Artif. Intell. ECAI 2021*, Jul. 2021.

[20] Gadiraju, H. K. V., V. R. Barry, and R. K. Jain, "Improved performance of PV water pumping system using dynamic reconfiguration algorithm under partial shading conditions," *CPSS Transactions on Power Electronics and Applications*, Vol. 7, No. 2, 206–215, 2022.

[21] Mahmood, A. S. and M. Teke, "Improving the efficiency of solar systems by tracking the MPP under different test conditions," *Progress In Electromagnetics Research B*, Vol. 99, 83–102, 2023.

[22] Priyadarshi, N., S. Padmanaban, M. S. Bhaskar, F. Blaabjerg, and J. B. Holm-Nielsen, "An improved hybrid PV-wind power system with MPPT for water pumping applications," *International Transactions on Electrical Energy Systems*, Vol. 30, No. 2, 1–26, 2020.

[23] Hilali, A., N. E. Ouanjli, S. Mahfoud, A. S. Al-Sumaiti, and M. A. Mossa, "Optimization of a solar water pumping system in varying weather conditions by a new hybrid method based on fuzzy logic and incremental conductance," *Energies*, Vol. 15, No. 22, 8518, 2022.

[24] Bjaoui, M., B. Khiari, R. Benadli, M. Memni, and A. Sellami, "Practical implementation of the backstepping sliding mode controller mppt for a PV-storage application," *Energies*, Vol. 12, No. 18, 3539, 2019.

[25] Villegas-Mier, C. G., J. Rodriguez-Resendiz, J. M. Álvarez Alvarado, H. Rodriguez-Resendiz, A. M. Herrera-Navarro, and O. Rodríguez-Abreo, "Artificial neural networks in MPPT algorithms for optimization of photovoltaic power systems: A review," *Micromachines*, Vol. 12, No. 10, 1–19, 2021.

[26] Ramaprabha, R., V. Gothandaraman, K. Kanimozhi, R. Divya, and B. L. Mathur, "Maximum power point tracking using GA-optimized artificial neural network for solar PV system," in *2011 1st International Conference on Electrical Energy Systems*, 264–268, 2011.

[27] Taouni, A., A. Abbou, M. Akherraz, A. Ouchatti, and R. Majdoul, "MPPT design for photovoltaic system using backstepping control with boost converter," in *2016 International Renewable and Sustainable Energy Conference (IRSEC)*, 469–475, 2016.

[28] Belkaid, A., J. P. Gaubert, and A. Gherbi, "An improved sliding mode control for maximum power point tracking in photovoltaic systems," *Journal of Control Engineering and Applied Informatics*, Vol. 18, No. 1, 86–94, 2016.

[29] "PV sistemler i çin M PPT kontrol cihazı tasarımı v e karşılaştırılması design and comparison of MPPT controller for PV systems," 2023.

[30] Sen, R., A. Garg, and A. Singh, "Modeling of PV array using P&O algorithm in boost converter," in *2017 International Conference on Computing and Communication Technologies for Smart Nation (IC3TSN)*, 231–236, 2017.

[31] Raj, A. and R. P. Praveen, "Highly efficient DC-DC boost converter implemented with improved MPPT algorithm for utility level photovoltaic applications," *Ain Shams Engineering Journal*, Vol. 13, No. 3, 101617, 2022.

[32] Fereka, D., M. Zerikat, and A. Belaidi, "MRAS sensorless speed control of an induction motor drive based on fuzzy sliding mode control," in *2018 7th International Conference on Systems and Control (ICSC)*, 230–236, 2018.

[33] Sharma, G., D. Parashar, and A. Chandel, "Analysis of dynamic model of three phase induction motor with matlab/simulink," in *2020 International Conference on Advances in Computing, Communication & Materials (ICACCM)*, 51–58, 2020.

[34] Sudaryanto, A., E. Purwanto, I. Ferdiansyah, S. D. Nugraha, O. A. Qudsi, M. M. Rifadil, and M. R. Rusli, "Design and implementation of SVPWM inverter to reduce total harmonic distortion (THD) on three phase induction motor speed regulation using constant V/F," in *2020 3rd International Seminar on Research of Information Technology and Intelligent Systems (ISRITI)*, 412–417, 2020.

[35] Hannan, M. A., J. A. Ali, P. J. Ker, A. Mohamed, M. S. H. Lipu, and A. Hussain, "Switching techniques and intelligent controllers for induction motor drive: issues and recommendations," *IEEE Access*, Vol. 6, 47 489–47 510, 2018.

[36] Harsha, A. R., S. Pranupa, B. M. K. Kumar, S. N. Rao, and M. S. Indira, "Arduino based V/F drive for a three phase induction motor using single phase supply," in *2020 International Conference on Smart Technologies in Computing, Electrical and Electronics (ICSTCEE)*, 90–94, 2020.

[37] Pena, J. M. and E. V. Diaz, "Implementation of V/F scalar control for speed regulation of a three-phase induction motor," in *Proc. 2016 IEEE ANDESCON*, 2017.